

Fundamental limits on the rate of bacterial cell division

³ Nathan M. Belliveau^{†, 1}, Griffin Chure^{†, 2, 3}, Christina L. Hueschen⁴, Hernan G.
⁴ Garcia⁵, Jané Kondev⁶, Daniel S. Fisher⁷, Julie Theriot^{1, 2, 8}, Rob Phillips^{1, 2, 9, *}

*For correspondence:

[†]These authors contributed equally to this work

⁵ Department of Biology, University of Washington, Seattle, WA, USA; ²Division of
⁶ Biology and Biological Engineering, California Institute of Technology, Pasadena, CA,
⁷ USA; ³Department of Applied Physics, California Institute of Technology, Pasadena, CA,
⁸ USA; ⁴Department of Chemical Engineering, Stanford University, Stanford, CA, USA;
⁹ Department of Molecular Cell Biology and Department of Physics, University of
¹⁰ California Berkeley, Berkeley, CA, USA; ⁶Department of Physics, Brandeis University,
¹¹ Waltham, MA, USA; ⁷Department of Applied Physics, Stanford University, Stanford, CA,
¹² USA; ⁸Allen Institute for Cell Science, Seattle, WA, USA; ⁹Department of Physics,
¹³ California Institute of Technology, Pasadena, CA, USA; *Contributed equally

14

15 Abstract

16

17 Introduction

18 The range of bacterial growth rates can be enormous. In natural environments, some microbial
¹⁹ organisms might double only once per year, whereas in comfortable laboratory conditions growth
²⁰ can be rapid with several divisions per hour. This remarkable diversity illustrates the intimate re-
²¹ lationship between environmental conditions and the rates at which cells convert nutrients into
²² new cellular material. This relationship between the environment and cellular growth rate has re-
²³ mained a major topic of inquiry in bacterial physiology for over a century (*Jun et al., 2018*). In 1958,
²⁴ Schaecter, Malløe, and Kjeldgaard reported the discovery of a logarithmic relationship between
²⁵ the total cellular protein content and the cellular growth rate, revealing a fundamental rela-
²⁶ tionship between the environment and the composition of the intracellular milieu (*Schaechter et al.,*
²⁷ *1958*).

28 Over the past decade, a remarkable body of work has reexamined this relationship with single-
²⁹ cell and single-protein resolution using modern methods of video microscopy (*Si et al., 2017; Har-*
³⁰ *riss and Theriot, 2018*) and through advances in mass spectrometry and sequencing technologies
³¹ (*Schmidt et al., 2016; Li et al., 2014*). This has permitted quantitative insight into how bacteria like
³² *E. coli* allocate their cellular resources under nutrient-limitation, and following genomic and phar-
³³ macological perturbations (*Scott et al., 2010; Hui et al., 2015; Basan et al., 2015*). This body of
³⁴ experimental data places us in the auspicious position to explore how the abundance of essential
³⁵ protein complexes are related to the growth rate of the population and interrogate what biological
³⁶ processes may set the speed limit of bacterial growth.

37 In this work, we seek to leverage a collection of proteomic data sets of *Escherichia coli* across 31
³⁸ growth conditions (*Valgepea et al., 2013; Li et al., 2014; Peebo et al., 2015; Hui et al., 2015; Schmidt*
³⁹ *et al., 2016*) to quantitatively explore what biological processes may set the speed limit of bacterial
⁴⁰ growth. Broadly speaking, we entertain several classes of hypotheses as are illustrated in *Figure 1*.
⁴¹ First, we consider potential limits on the transport of nutrients into the cell. We address this hy-

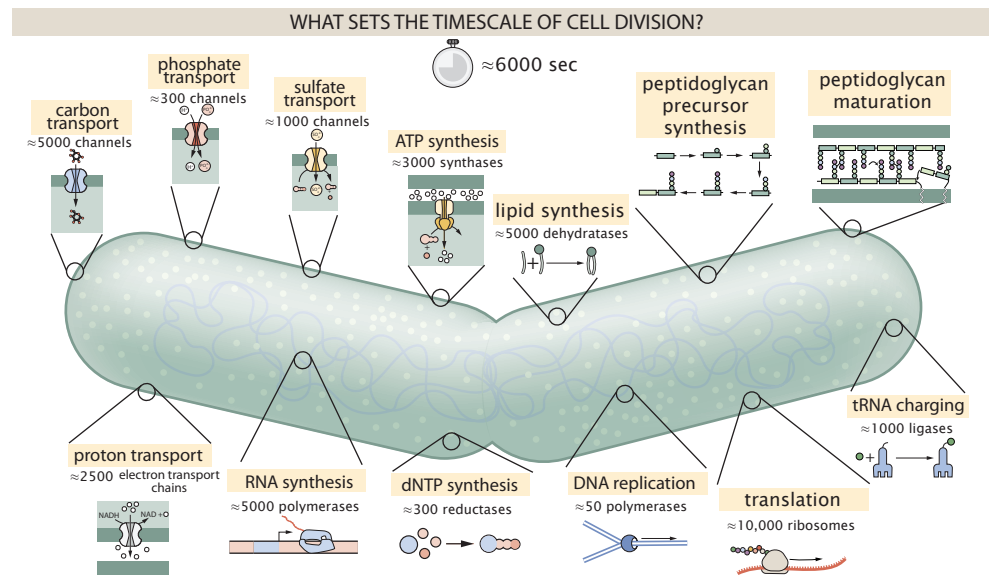


Figure 1. Transport and synthesis processes necessary for cell division. We consider an array of processes necessary for a cell to double its molecular components. Such processes include the transport of carbon across the cell membrane, the production of ATP, and fundamental processes of the central dogma namely RNA, DNA, and protein synthesis. A schematic of each synthetic or transport category is shown with an estimate of the rate per macromolecular complex. In this work, we consider a standard bacterial division time of ≈ 6000 sec.

42 pothesis by performing an order-of-magnitude estimate for how many carbon atoms needed to
 43 facilitate this requirement given a 6000 second division time. As a second hypothesis, we consider
 44 the possibility that there exists a fundamental limit on how quickly the cell can generate ATP. We ap-
 45 proach this hypothesis from two angles, considering how many ATP synthase complexes must be
 46 needed to churn out enough ATP to power protein translation followed by an estimation of how
 47 many electron transport complexes must be present to maintain the proton motive force. Our
 48 third and final class of hypotheses centers on the synthesis of a variety of biomolecules. Our focus
 49 is primarily on the stages of the central dogma as we estimate the number of protein complexes
 50 needed for DNA replication, transcription, and protein translation.

51 With estimates in hand for each of these processes, we turn to our collection of data sets to
 52 assess the accuracy of our estimates. In broad terms, we find that the majority of our estimates are
 53 in line with experimental observations, with protein copy numbers apparently well-tuned for the
 54 task of cell doubling. This allows us to systematically scratch off the hypotheses diagrammed in **Fig-**
55 ure 1 as setting possible speed limits. Ultimately, we find that protein translation (particularly the
 56 generation of new ribosomes) acts as 1) a rate limiting step for the *fastest* bacterial division, and 2)
 57 the major determinant of bacterial growth across all nutrient conditions we have considered under
 58 steady state, exponential growth. This perspective is in line with the linear correlation observed
 59 between growth rate and ribosomal content (usually quantified through the ratio of RNA to pro-
 60 tein) for fast growing cells (*Scott et al., 2010*), but suggests a more prominent role for ribosomes
 61 in setting the doubling time across all conditions of nutrient limitation. Here we again leverage the
 62 quantitative nature of this data set and present a quantitative model of the relationship between
 63 the fraction of the proteome devoted to ribosomes and the speed limit of translation, revealing
 64 a fundamental tradeoff between the translation capacity of the ribosome pool and the maximal
 65 growth rate.

66 Nutrient Transport

67 In order to build new cellular mass, the molecular and elemental building blocks must be scav-
 68 enged from the environment in different forms. Carbon, for example, is acquired via the transport
 69 of carbohydrates and sugar alcohols with some carbon sources receiving preferential treatment
 70 in their consumption (*Monod, 1947*). Phosphorus, sulfur, and nitrogen, on the other hand, are
 71 harvested primarily in the forms of inorganic salts, namely phosphate, sulfate, and ammonia (*Jun*
 72 *et al., 2018; Assentoft et al., 2016; Stasi et al., 2019; Antonenko et al., 1997; Rosenberg et al., 1977;*
 73 *Willsky et al., 1973*). All of these compounds have different permeabilities across the cell mem-
 74 brane and most require some energetic investment either via ATP hydrolysis or through the pro-
 75 ton electrochemical gradient to bring the material across the hydrophobic cell membrane. Given
 76 the diversity of biological transport mechanisms and the vast number of inputs needed to build a
 77 cell, we begin by considering transport of elemental requirements as a possible rate-limiting step
 78 of bacterial cell division.

79 The elemental composition of *E. coli* has received much quantitative attention over the past
 80 half century (*Neidhardt et al., 1991; Taymaz-Nikerel et al., 2010; Heldal et al., 1985; Bauer and Ziv,*
 81 *1976*), providing us with a starting point for estimating the copy numbers of various transporters.
 82 While there is some variability in the exact elemental percentages (with different uncertainties), we
 83 can estimate that the dry mass of a typical *E. coli* cell is $\approx 45\%$ carbon (BNID: 100649, *Milo et al.*
 84 (*2010*)), $\approx 15\%$ nitrogen (BNID: 106666, *Milo et al. (2010)*), $\approx 3\%$ phosphorus (BNID: 100653, *Milo*
 85 *et al. (2010)*), and 1% sulfur (BNID: 100655, *Milo et al. (2010)*). In the coming paragraphs, we will
 86 examine how many transporters and/or channels must be present to maintain these elemental
 87 compositions with a moderate doubling time of 6,000 s.

88 Carbon Transport

89 We begin with the most abundant element by mass, carbon. Using ≈ 0.3 pg as the typical *E. coli*
 90 dry mass (BNID: 103904, *Milo et al. (2010)*), we estimate that $\approx 10^{10}$ carbon atoms must be brought
 91 into the cell in order to double all of the carbon-containing molecules (*Figure 2(A, top)*). Typical
 92 laboratory growth conditions, such as those explored in the aforementioned proteomic data sets,
 93 provide carbon as single class of sugar such as glucose, galactose, or xylose to name a few. *E.*
 94 *coli* has evolved myriad mechanisms by which these sugars can be transported across the cell
 95 membrane. One such mechanism of transport is via the PTS system which is a highly modular
 96 system capable of transporting a diverse range of sugars (*Escalante et al., 2012*). The glucose-
 97 specific component of this system transports ≈ 200 glucose molecules per second per channel
 98 (BNID: 114686, *Milo et al. (2010)*). Making the assumption that this is a typical sugar transport rate,
 99 coupled with the need to transport 10^{10} carbon atoms, we arrive at the conclusion that on the
 100 order of 1,000 transporters must be expressed in order to bring in enough carbon atoms to divide
 101 in 6,000 s, diagrammed in the top panel of *Figure 2(A)*. This estimate, along with the observed
 102 average number of carbohydrate transporters present in the proteomic data sets (*Schmidt et al.,*
 103 *2016; Peebo et al., 2015; Valgepea et al., 2013; Li et al., 2014*), is shown in *Figure 2(A)*. While we
 104 estimate 1,000 transporters are needed, the data reveals that at a division time of $\approx 6,000$ s there is
 105 nearly a ten-fold excess of transporters. Furthermore, the data illustrates that the average number
 106 of carbohydrate transporters present is largely-growth rate independent.

107 The estimate presented in *Figure 2(A)* neglects any specifics of the regulation of carbon trans-
 108 port system and presents a data-averaged view of how many carbohydrate transporters are present
 109 on average. Using the diverse array of growth conditions explored in the proteomic data sets,
 110 we can explore how individual carbon transport systems depend on the population growth rate.
 111 In *Figure 2(B)*, we show the total number of carbohydrate transporters specific to different car-
 112 bon sources. A striking observation, shown in the top-left plot of *Figure 2(B)*, is the constancy
 113 in the expression of the glucose-specific transport systems (the PtsG enzyme of the PTS system
 114 and the glucose-transporting ManXYZ complex). Additionally, we note that the total number of
 115 glucose-specific transporters is tightly distributed $\approx 10^4$ per cell, an order of magnitude beyond

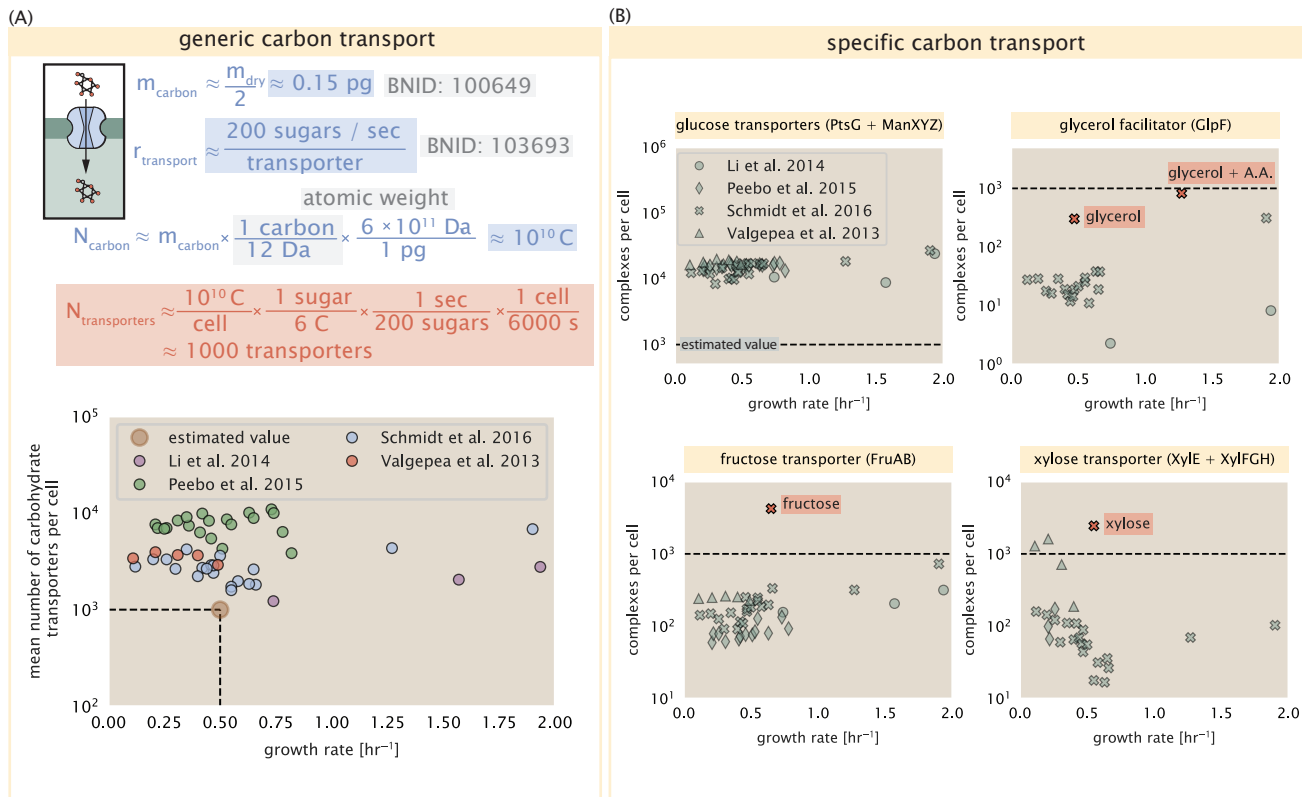


Figure 2. The abundance of carbon transport systems across growth rates. (A) A simple estimate for the minimum number of generic carbohydrate transport systems (top) assumes $\approx 10^{10}$ C are needed to complete division, each transported sugar contains ≈ 6 C, and each transporter conducts sugar molecules at a rate of ≈ 200 per second. Bottom plot shows the estimated number of transporters needed at a growth rate of ≈ 0.5 per hr (light-brown point and dashed lines). Colored points correspond to the mean number of carbohydrate transporters for different growth conditions across different published datasets. (B) The abundance of various specific carbon transport systems plotted as a function of the population growth rate. Red points and red-highlighted text indicate conditions in which the only source of carbon in the growth medium induces expression of the transport system.

116 the estimate shown in **Figure 2(A)**. This illustrates that *E. coli* maintains a substantial number of
 117 complexes present for transporting glucose which is known to be the preferential carbon source
 118 (**Monod, 1947; Liu et al., 2005; Aidelberg et al., 2014**).

119 It is now understood that a large number of metabolic operons are regulated with dual-input
 120 logic gates that are only expressed when glucose concentrations are low (mediated by cyclic-AMP
 121 receptor protein CRP) and the concentration of other carbon sources are elevated (**Gama-Castro**
 122 **et al., 2016; Zhang et al., 2014b**). A famed example of such dual-input regulatory logic is in the regu-
 123 lation of the *lac* operon which is only natively activated in the absence of glucose and the presence
 124 of allolactose, an intermediate in lactose metabolism (**Jacob and Monod, 1961**), though we now
 125 know of many other such examples (**Ireland et al., 2020; Gama-Castro et al., 2016; Belliveau et al.,**
 126 **2018**). This illustrates that once glucose is depleted from the environment, cells have a means to
 127 dramatically increase the abundance of the specific transporter needed to digest the next sugar
 128 that is present. Several examples of induced expression of a specific carbon-source transporters
 129 are shown in **Figure 2(B)**. Points colored in red (labeled by red text-boxes) correspond to growth
 130 conditions in which the specific carbon source (glycerol, xylose, or fructose) is present. These plots
 131 show that, in the absence of the particular carbon source, expression of the transporters is main-
 132 tained on the order of $\sim 10^2$ per cell. However, when induced, the transporters become highly-
 133 expressed and are present on the order of $\sim 10^4$ per cell, which exceeds the generic estimate given
 134 in **Figure 2(A)**. Together, this generic estimation and the specific examples of induced expression
 135 suggest that transport of carbon across the cell membrane, while critical for growth, is not the
 136 rate-limiting step of cell division.

137 In the context of speeding up growth, one additional limitation is the fact that the cell's inner
 138 membrane is occupied by a multitude of other membrane proteins. Considering a rule-of-thumb
 139 for the surface area of *E. coli* of about $6 \mu\text{m}^2$ (BNID: 101792, **Milo et al. (2010)**), we expect an areal
 140 density for 1,000 transporters to be approximately 200 transporters/ μm^2 . For a glucose trans-
 141 porter occupying about $50 \text{ nm}^2/\text{dimer}$, this amounts to about only 1 percent of the total inner
 142 membrane (**Szenk et al., 2017**). In addition, bacterial cell membranes typically have densities of
 143 10^5 proteins/ μm^2 (**Phillips, 2018**), implying that the cell could accommodate more transporters if
 144 it were rate limiting.

145 **Phosphorus and Sulfur Transport**

146 We now turn our attention towards other essential elements, namely phosphorus and sulfur. Phos-
 147 phorus is critical to the cellular energy economy in the form of high-energy phosphodiester bonds
 148 making up DNA, RNA, and the NTP energy pool as well as playing a critical role in the post-translational
 149 modification of proteins and defining the polar-heads of lipids. In total, phosphorus makes up
 150 $\approx 3\%$ of the cellular dry mass which in typical experimental conditions is in the form of inorganic
 151 phosphate. The cell membrane has remarkably low permeability to this highly-charged and critical
 152 molecule, therefore requiring the expression of active transport systems. In *E. coli*, the proton elec-
 153 trochemical gradient across the inner membrane is leveraged to transport inorganic phosphate
 154 into the cell (**Rosenberg et al., 1977**). Proton-solute symporters are widespread in *E. coli* (**Ramos and**
 155 **Kaback, 1977; Booth et al., 1979**) and can have rapid transport rates of 50 molecules per second
 156 for sugars and other solutes (BNID: 103159; 111777, **Milo et al. (2010)**). In *E. coli* the PitA phosphate
 157 transport system has been shown to very tightly coupled with the proton electrochemical gradient
 158 with a 1:1 proton:phosphate stoichiometric ratio (**Harris et al., 2001; Feist et al., 2007**). Illustrated
 159 in **Figure 3(A)**, we can estimate that ≈ 300 phosphate transporters are necessary to maintain an
 160 $\approx 3\%$ dry mass with a 6,000 s division time. This estimate is again satisfied when we examine the
 161 observed copy numbers of PitA in proteomic data sets (plot in **Figure 3(A)**). While our estimate is
 162 very much in line with the observed numbers, we emphasize that this is likely a slight over estimate
 163 of the number of transporters needed as there are other phosphorous scavenging systems, such
 164 as the ATP-dependent phosphate transporter Pst system which we have neglected.

165 Satisfied that there are a sufficient number of phosphate transporters present in the cell, we

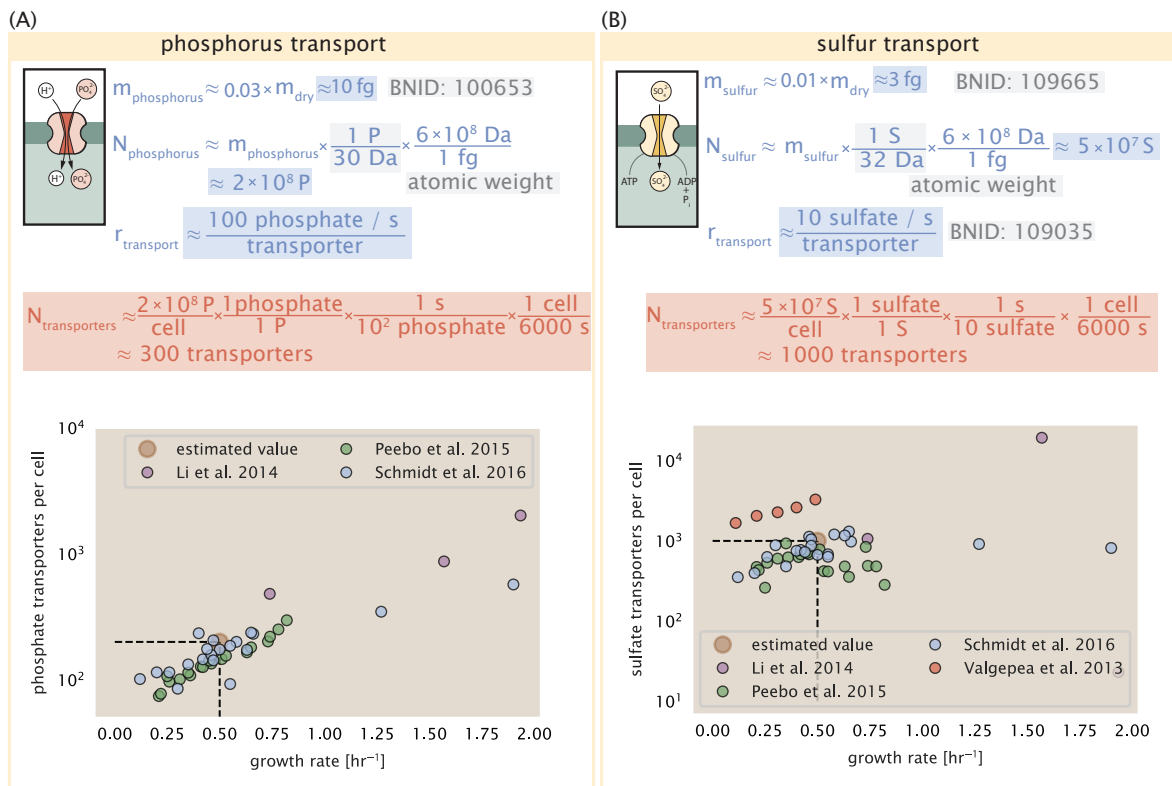


Figure 3. Estimates and measurements of phosphate and sulfate transport systems as a function of growth rate. (A) Estimate for the number of PitA phosphate transport systems needed to maintain a 3% phosphorus *E. coli* dry mass. Points in plot correspond to the total number of PitA transporters per cell. (B) Estimate of the number of CysUWA complexes necessary to maintain a 1% sulfur *E. coli* dry mass. Points in plot correspond to average number of CysUWA transporter complexes that can be formed given the transporter stoichiometry $[\text{CysA}]_2[\text{CysU}][\text{CysW}][\text{Sbp/CysP}]$.

now turn sulfur transport as another potentially rate limiting process. Similar to phosphate, sulfate is highly-charged and not particularly membrane permeable, requiring active transport. While there exists a $\text{H}^+/\text{SO}_4^{2-}$ symporter in *E. coli*, it is in relatively low abundance and is not well characterized (Zhang et al., 2014a). Sulfate is predominantly acquired via the ATP-dependent ABC transporter CysUWA system which also plays an important role in selenium transport (Sekowska et al., 2000; Sirko et al., 1995). While specific kinetic details of this transport system are not readily available, generic ATP transport systems in prokaryotes are on the order of 1 to 10 molecules per second (BNID: 109035, Milo et al. (2010)). Combining this generic transport rate, measurement of sulfur comprising 1% of dry mass, and a 6,000 second division time yields an estimate of ≈ 1000 CysUWA complexes per cell (Figure 3(B)). Once again, this estimate is in notable agreement with proteomic data sets, suggesting that there are sufficient transporters present to acquire the necessary sulfur. In a similar spirit of our estimate of phosphorus transport, we emphasize that this is likely an overestimate of the number of necessary transporters as we have neglected other sulfur scavenging systems that are in lower abundance.

180 Nitrogen Transport

Finally, we turn to nitrogen transport as the last remaining transport system highlighted in Figure 1. Unlike phosphate, sulfate, and various sugar molecules, nitrogen in the form of ammonia can readily diffuse across the cell membrane and has a permeability on par with water ($\approx 10^5 \text{ nm/s}$, BNID:110824 Milo et al. (2010)). In particularly nitrogen-poor conditions, *E. coli* expresses a transporter (AmtB) which appears to aid in nitrogen assimilation, though the mechanism and kinetic

186 details of transport is still a matter of debate (*van Heeswijk et al., 2013; Khademi et al., 2004*). Be-
 187 yond ammonia, another plentiful source of nitrogen come in the form of glutamate, which has it's
 188 own complex metabolism and scavenging pathways. However, nitrogen is plentiful in the growth
 189 conditions examined in this work, permitting us to neglect nitrogen transport as a potential rate
 190 limiting process in cell division.

191 Energy Production

192 While the transport of nutrients is required to build new cell mass, the metabolic pathways in-
 193 volved in assimilation both consumes and generates energy in the form of NTPs. The high-energy
 194 phosphodiester bonds of (primarily) ATP power a variety of cellular processes that drive biological
 195 systems away from thermodynamic equilibrium. Our next class of estimates consider the energy
 196 budget of a dividing cell in terms of the synthesis of ATP from ADP and inorganic phosphate as well
 197 as maintenance of the electrochemical proton gradient which powers it.

198 ATP Synthesis

199 Hydrolysis of the terminal phosphodiester bond of ATP forming ADP and an inorganic phosphate is
 200 a kinetic driving force in a wide array of biochemical reactions. One such reaction is the formation
 201 of peptide bonds during translation which requires ≈ 2 ATPs for the charging of an amino acid
 202 to the tRNA and ≈ 2 ATP equivalents for the formation of the peptide bond between amino acids.
 203 Together, these energetic costs consume $\approx 80\%$ of the cells ATP budget (BNID: 107782; 106158;
 204 101637; 111918, *Milo et al. (2010)*). The pool of ATP is produced by the F_1 - F_0 ATP synthase – a
 205 membrane-bound rotary motor which under ideal conditions can yield ≈ 300 ATP per second (BNID:
 206 114701; *Milo et al. (2010); Weber and Senior (2003)*).

207 To estimate the total number of ATP equivalents consumed during a cell cycle, we will make
 208 the approximation that there are $\approx 3 \times 10^6$ proteins per cell with an average protein length of ≈ 300
 209 peptide bonds (BNID: 115702; 108986; 104877, *Milo et al. (2010)*). Taking these values together,
 210 we estimate that the typical *E. coli* cell consumes $\approx 5 \times 10^9$ ATP per cell cycle on protein synthesis
 211 alone and $\approx 6 \times 10^9$ ATP in total. Assuming that the ATP synthases are operating at their fastest
 212 possible rate, ≈ 3000 ATP synthases are needed to keep up with the energy demands of the cell.
 213 This estimate and a comparison with the data are shown in *Figure 4* (A). Despite our assumption
 214 of maximal ATP production rate per synthase and approximation of all NTP consuming reactions
 215 being the same as ATP, we find that an estimate of a few thousand complete synthases per cell to
 216 agree well with the experimental data.

217 Generating the Proton Electrochemical Gradient

218 In order to produce ATP, the F_1 - F_0 ATP synthase itself must consume energy. Rather than burning
 219 through its own product, this intricate macromolecular machine has evolved to exploit the elec-
 220 trochemical potential established across the inner membrane through cellular respiration. This
 221 electrochemical gradient is manifest by the pumping of protons into the intermembrane space via
 222 the electron transport chains as they reduce NADH. In *E. coli*, this potential difference is ≈ -200
 223 mV (BNID: 102120, *Milo et al. (2010)*). As estimated in the supporting information, this potential
 224 difference is generated by maintaining $\approx 2 \times 10^4$ protons in the intermembrane space.

225 However, the constant rotation of the ATP synthases would rapidly abolish this potential differ-
 226 ence if it were not being actively maintained. To undergo a complete rotation (and produce a single
 227 ATP), the F_1 - F_0 ATP synthase must shuttle ≈ 4 protons across the membrane into the cytosol (BNID:
 228 103390, *Milo et al. (2010)*). With ≈ 3000 ATP synthases each generating 300 ATP per second, the
 229 2×10^4 protons establishing the 200 mV potential would consumed in only a few milliseconds. This
 230 brings us to our next estimate: how many electron transport complexes are needed to support
 231 the consumption rate of the ATP synthases?

232 The electrochemistry of the electron transport complexes of *E. coli* have been the subject of
 233 intense biochemical and biophysical study over the past half century (*Ingledew and Poole, 1984*;

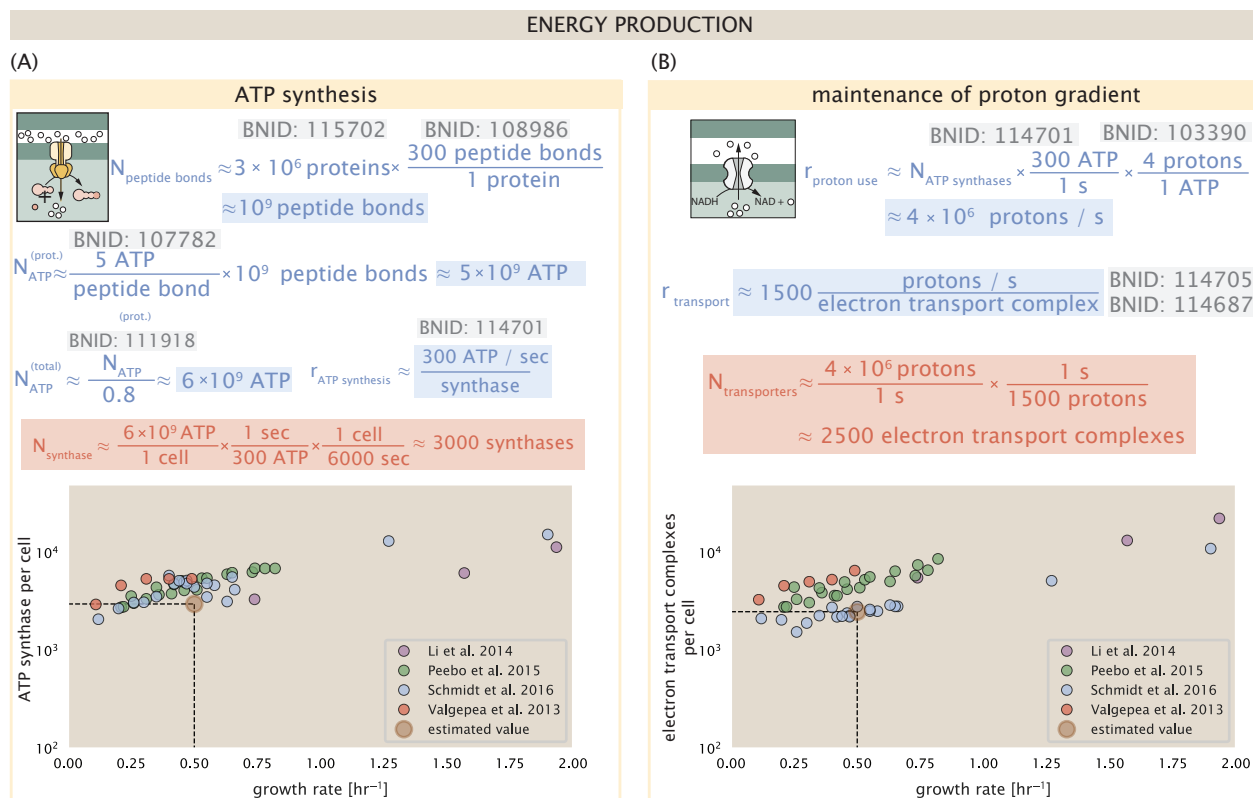


Figure 4. The abundance of F₁-F₀ ATP synthases and electron transport chain complexes as a function of growth rate. (A) Estimate of the number of F₁-F₀ ATP synthase complexes needed accommodate peptide bond formation and other NTP dependent processes. Points in plot correspond to the mean number of complete F₁-F₀ ATP synthase complexes that can be formed given proteomic measurements and the subunit stoichiometry [AtpE]₁₀[AtpF]₂[AtpB][AtpC][AtpH][AtpA]₃[AtpG][AtpD]₃. (B) Estimate of the number of electron transport chain complexes needed to maintain a membrane potential of ~ -200 mV given estimate of number of F₁-F₀ ATP synthases from (A). Points in plot correspond to the average number of complexes identified as being involved in aerobic respiration by the Gene Ontology identifier GO:0019646 that could be formed given proteomic observations. These complexes include cytochromes *bd1* ([CydA][CydB][CydX][CydH]), *bdII* ([AppC][AppB]), *bo3*, ([CyoD][CyoA][CyoB][CyoC]) and NADH:quinone oxioreducase I ([NuoA][NuoH][NuoJ][NuoK][NuoL][NuoM][NuoN][NuoB][NuoC][NuoE][NuoF][NuoG][NuoI]) and II ([Ndh]).

234 **Khademian and Imlay, 2017; Cox et al., 1970; Henkel et al., 2014.** A recent work (Szenk et al.,
 235 2017) examined the respiratory capacity of the *E. coli* electron transport complexes using structural
 236 and biochemical data, revealing that each electron transport chain rapidly pumps protons into the
 237 intermembrane space at a clip of ≈ 1500 protons per second (BNID: 114704; 114687, Milo et al.
 238 (2010)). Using our estimate of the number of ATP synthases required per cell (Figure 4(A)), coupled
 239 with these recent measurements, we estimate that ≈ 1000 electron transport complexes would be
 240 necessary to facilitate the $\approx 4 \times 10^6$ protons per second diet of the cellular ATP synthases. This
 241 estimate is in agreement with the number of complexes identified in the proteomic datasets (plot
 242 in Figure 4(B)).

243 Energy Production in a Crowded Membrane.

244 For each protein considered so far, the data shows that in general their numbers increase with
 245 growth rate. This is in part a consequence of the increase in cell length and width at that is common
 246 to many rod-shaped bacteria at faster growth rates (Ojikic et al., 2019; Harris and Theriot, 2018).
 247 For the particular case of *E. coli*, the total cellular protein and cell size increase logarithmically
 248 with growth rate (Schaechter et al., 1958; Si et al., 2017). Indeed, this is one reason why we have
 249 considered only a single, common growth condition across all our estimates so far. Such a scaling

250 will require that the total number of proteins and net demand on resources also grow in proportion
 251 to the increase in cell size divided by the cell's doubling time. Recall however that each transport
 252 process, as well as the ATP production via respiration, is performed at the bacterial membrane.
 253 This means that their maximum productivity can only increase in proportion to the cell's surface
 254 area divided by the cell doubling time. This difference in scaling would vary in proportion to the
 255 surface area-to-volume (S/V) ratio.

256 While we found that there was more than sufficient membrane real estate for carbon intake in
 257 our earlier estimate, the total number of ATP synthases and electron chain transport complexes
 258 both exhibit a clear increase in copy number with growth rate, reaching in excess of 10^4 copies per
 259 cell (**Figure 4**). Here we consider the consequences of this S/V ratio scaling in more detail.

260 In our estimate of ATP production above we found that a cell demands about 6×10^9 ATP or
 261 10^6 ATP/s. With a cell volume of roughly 1 fL, this corresponds to about 2×10^{10} ATP per fL of cell
 262 volume, in line with previous estimates (*Stouthamer and Bettenhausen, 1977; Szenk et al., 2017*).
 263 In **Figure 5** (A) we plot this ATP demand as a function of the S/V ratio in green, where we have
 264 considered a range of cell shapes from spherical to rod-shaped with an aspect ratio (length/width)
 265 equal to 4 (See appendix for calculations of cell volume and surface area). In order to consider the
 266 maximum power that could be produced, we consider the amount of ATP that can be generated by a
 267 membrane filled with ATP synthase and electron transport complexes, which provides a maximal
 268 production of about 3 ATP / (nm²·s) (*Szenk et al., 2017*). This is shown in red in **Figure 5**(A), which
 269 shows that at least for the growth rates observed, the energy demand is roughly an order of mag-
 270 nitude less. Interestingly, *Szenk et al.* (2017) also found that ATP production by respiration is less
 271 efficient than by fermentation per membrane area occupied due to the additional proteins of the
 272 electron transport chain. This suggests that even under anaerobic growth, there will be sufficient
 273 membrane space for ATP production in general.

274 While this serves to highlight the diminishing capacity to provide resources to grow if the cell
 275 increases in size (and its S/V decreases), the blue region in **Figure 5**(A) represents a somewhat
 276 unachievable limit since the inner membrane must also include other proteins such as those re-
 277 quired for lipid and membrane synthesis. To gain insight, we used the proteomic data to look at
 278 the distribution of proteins on the inner membrane. Here we use Gene Ontology (GO) annotations
 279 (*Ashburner et al., 2000; The Gene Ontology Consortium, 2018*) to identify all proteins embedded
 280 or peripheral to the inner membrane (GO term: 0005886). Those associated but not membrane-
 281 bound include proteins like MreB and FtsZ, that traverse the inner membrane by treadmilling and
 282 must nonetheless be considered as a vital component occupying space on the membrane. In **Fig-**
 283 **ure 5** (B), we find that the total protein mass per μm^2 is relatively constant with growth rate. Inter-
 284 estingly, when we consider the distribution of proteins grouped by their Clusters of Orthologous
 285 Groups (COG) (*Tatusov et al., 2000*), the relative abundance for those in metabolism (including ATP
 286 synthesis via respiration) is also relatively constant.

287 **Synthesis of the Cell Wall and lipid membrane.**

288 [To be completed.]

289 **Function of the Central Dogma**

290 Up to this point, we have considered a variety of transport and biosynthetic processes that are
 291 critical to acquiring and generating new cell mass. While there are of course many other metabolic
 292 processes we could consider and perform estimates of (such as the components of fermentative
 293 versus aerobic respiration), we now turn our focus to some of the most central processes which
 294 *must* be undertaken irrespective of the growth conditions – the processes of the central dogma.

295 **DNA**

296 Most bacteria (including *E. coli*) harbor a single, circular chromosome and can have extra-chromosomal
 297 plasmids ~ 100 kbp in length. We will focus our quantitative thinking solely on the chromosome

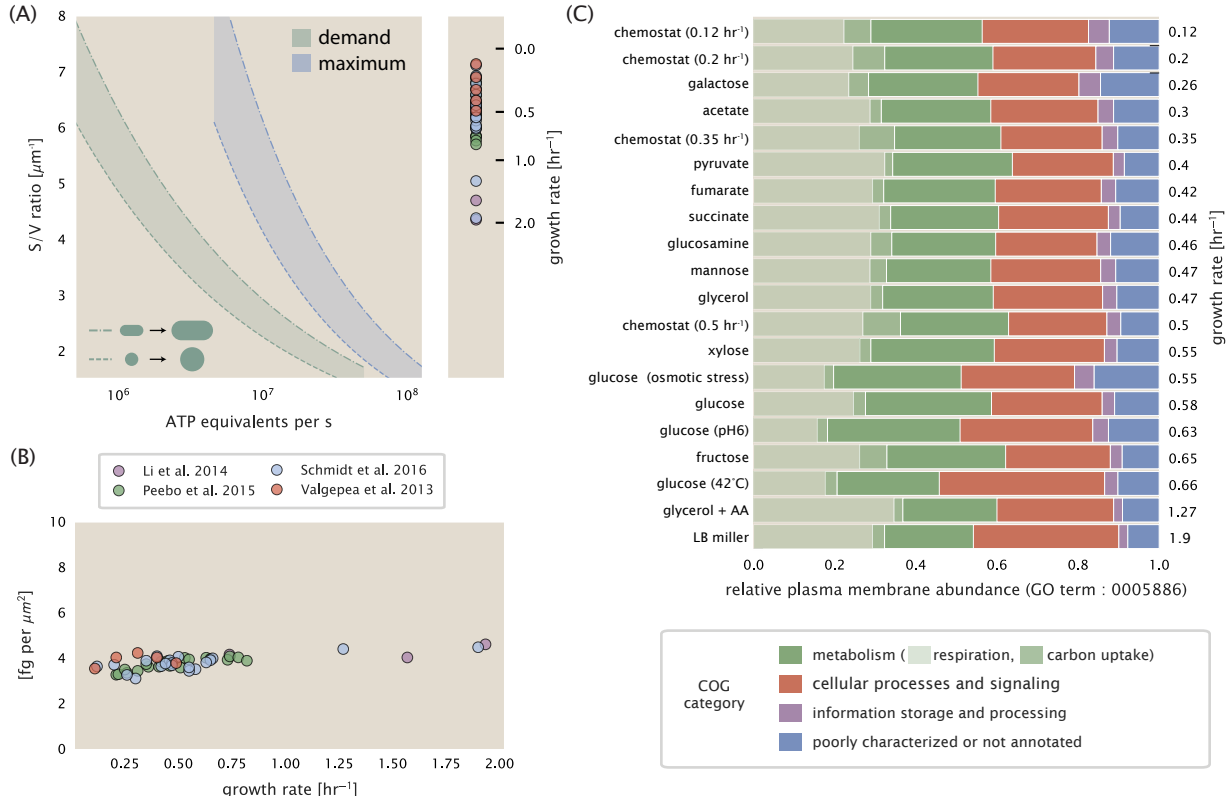


Figure 5. Influence of cell size and S/V ratio on ATP production and inner membrane composition. (A) Scaling of ATP demand and maximum ATP production as a function of S/V ratio. Cell volumes of 0.5 fL to 50 fL were considered, with the dashed (—) line corresponding to a sphere and the dash-dot line (---) reflecting a rod-shaped bacterium like *E. coli* with aspect ratio (length / width) of 0.4. Approximately 50% of the bacterial inner membrane is assumed to be protein, with the remainder lipid. (B) Total protein mass calculated for proteins with inner membrane annotation (GO term: 0005886). (C) Relative protein abundances by mass based on COG annotation. Metabolic proteins are further separated into respiration (F_1 - F_0 ATP synthase, NADH dehydrogenase I, succinate:quinone oxidoreductase, cytochrome b_{o3} ubiquinol oxidase, cytochrome bd -I ubiquinol oxidase) and carbohydrate transport (GO term: GO:0008643). Note that the elongation factor EF-Tu can also associate with the inner membrane, but was excluded in this analysis due to its high relative abundance (roughly identical to the total mass shown in part (B)).

298 of *E. coli* which harbors \approx 5000 genes and \approx 5×10^6 base pairs. To successfully divide and produce
 299 viable progeny, this chromosome must be faithfully replicated and segregated into each nascent
 300 cell. We again rely on the near century of literature in molecular biology to provide some insight
 301 towards the rates and mechanics of the replicative feat as well as the production of the replication
 302 starting materials, dNTPs.

303 dNTP synthesis

304 We begin our exploration of the DNA replicative processes by examining the production of the de-
 305 oxyribonucleotide triphosphates (dNTPs). The four major dNTPS (dATP, dTTP, dCTP, and dGTP) are
 306 synthesized *de novo* in separate pathways, requiring different building blocks. However, a critical
 307 step present in all dNTP synthesis pathways is the conversion from ribonucleotide to deoxyribonu-
 308 cleotide via the removal of the 3' hydroxyl group of the ribose ring (Rudd et al., 2016). This reaction
 309 is mediated by a class of enzymes termed ribonucleotide reductases, of which *E. coli* possesses
 310 two aerobically active complexes (termed I and II) and a single anaerobically active enzyme. Due to
 311 their peculiar formation of a radical intermediate, these enzymes have received much biochemical,
 312 kinetic, and structural characterization. One such work (Ge et al., 2003) performed a detailed *in*
 313 *vitro* measurement of the steady-state kinetic rates of these complexes, revealing a turnover rate
 314 of \approx 10 per second.

315 Considering this reaction (mediated by the ribonucleotide reductase complexes I and II) is cen-
 316 tral to synthesis of all dNTPS, it is reasonable to consider the abundance of these complexes as a
 317 measure of the total dNTP production in *E. coli*. Illustrated schematically in Figure 6 (A), we consider
 318 the fact that to replicate the cell's genome, on the order of \approx 10^7 dNTPs must be synthesized. As
 319 suming a production rate of 10 per second per ribonucleotide reductase complex and a cell division
 320 time of 6000 seconds, we arrive at an estimate of \approx 150 complexes are needed per cell. As shown
 321 in the bottom panel of Figure 6 (A), this estimate agrees with the experimental measurements of
 322 these complexes abundances within \approx 1/2 an order of magnitude.

323 Recent work has revealed that during replication, the ribonucleotide reductase complexes co-
 324 alesce to form discrete foci colocalized with the DNA replisome complex (Sánchez-Romero et al.,
 325 2011). This is particularly pronounced in environments where growth is slow, indicating that spatial
 326 organization and regulation of the activity of the complexes plays an important role.

327 DNA Replication

328 We now turn our focus towards the process of integration of the dNTP building blocks into the
 329 replicated chromosome strand via the DNA polymerase enzymes. Replication of bacterial chro-
 330 mosomes is initiated at a single region of the chromosome termed the *oriC* locus at which a pair
 331 of DNA polymerases bind and begin their high-fidelity replication of the genome in opposite di-
 332 rections. Assuming equivalence between the two replication forks, this means that the two DNA
 333 polymerase complexes (termed replisomes) meet at the midway point of the circular chromosome
 334 termed the *ter* locus. This division of labor means The kinetics of the five types of DNA polymerases
 335 (I – V) have been intensely studied, revealing that DNA polymerase III performs the high fidelity pro-
 336 cessive replication of the genome with the other "accessory" polymerases playing auxiliary roles
 337 (Fijalkowska et al., 2012). *In vitro* measurements have shown that DNA Polymerase III copies DNA
 338 at a rate of \approx 600 nucleotides per second (BNID: 104120, Milo et al. (2010)). Therefore, to replicate a
 339 single chromosome, two DNA polymerases replicating at their maximal rate would copy the entire
 340 genome in \approx 4000 s. Thus, with a division time of 6000 s (our "typical" growth rate for the purposes
 341 of this work), there is sufficient time for a pair of DNA polymerase III complexes to replicate the
 342 entire genome. However, this estimate implies that 4000 s would be the upper-limit time scale for
 343 bacterial division which is at odds with the familiar \approx 1500 s doubling time of *E. coli* in rich medium.

344 It is known well known that *E. coli* can parallelize its DNA replication such that multiple chromo-
 345 somes are being replicated at once. Recent work (Si et al., 2017) has shown that the replicative
 346 timescale of cell division can be massively parallelized where *E. coli* can have on the order of 10 -

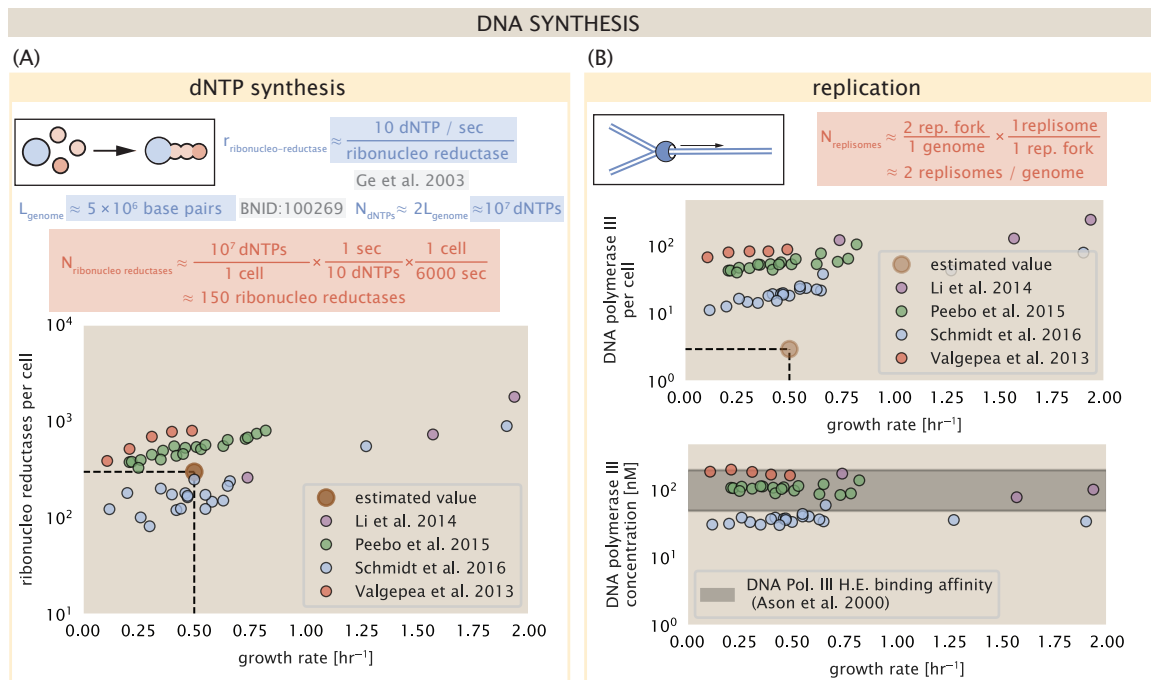


Figure 6. Complex abundance estimates for dNTP synthesis and DNA replication. (A) Estimate of the number of ribonucleotide reductase enzymes needed to facilitate the synthesis of $\approx 10^7$ dNTPs over the course of a 6000 second generation time. Points in the plot correspond to the total number of ribonucleotide reductase I ($[NrdA]_2[NrdB]_2$) and ribonucleotide reductase II ($[NrdE]_2[NrdF]_2$) complexes. (B) An estimate for the minimum number of DNA polymerase holoenzyme complexes needed to facilitate replication of a single genome. Points in the top plot correspond to the total number of DNA polymerase III holoenzyme complexes ($[DnaE]_3[DnaQ]_3[HolE]_3[DnaX]_5[HolB][HolA][DnaN]_4[HolC]_4[HolD]_4$) per cell. Bottom plot shows the effective concentration of DNA polymerase III holoenzyme given cell volumes calculated from the growth rate as in *Si et al. (2019)*.

347 12 replication forks at a given time. Thus, even in rapidly growing cultures, only a few polymerases
 348 (≈ 10) are needed to replicate the chromosome. However, as shown in **Figure 6(B)**, DNA polymerase
 349 III is nearly an order of magnitude more abundant. This discrepancy can be understood
 350 when considering the binding affinities. The DNA polymerase III complex is highly processive, fa-
 351 cilitated by a strong affinity of the complex to the DNA. *In vitro* biochemical characterization has
 352 quantified the K_D of DNA polymerase III holoenzyme to single-stranded and double-stranded DNA
 353 to be 50 and 200 nM, respectively (**Ason et al., 2000**). The bottom plot in **Figure 6 (B)** shows that
 354 the concentration of the DNA polymerase III across all data sets and growth conditions is within
 355 this range. Thus, while the copy number of the DNA polymerase III is in excess of the strict num-
 356 ber required to replicate the genome, the copy number is tuned such that the concentration is
 357 approximately equal to the dissociation constant to the DNA. While the processes regulating the
 358 initiation of DNA replication are complex and involve more than just the holoenzyme, these data
 359 indicate that the kinetics of replication rather than the explicit copy number of the DNA polymerase
 360 III holoenzyme is the more relevant feature of DNA replication to consider.

361 RNA Synthesis

362 With the machinery governing the replication of the genome accounted for, we now turn our atten-
 363 tion to the next stage of the central dogma – the transcription of DNA to form RNA. We primarily
 364 consider three major groupings of RNA, namely the RNA associated with ribosomes (rRNA), the
 365 RNA encoding the amino-acid sequence of proteins (mRNA), and the RNA which links codon se-
 366 quence to amino-acid identity during translation (tRNA). Despite the varied function of these RNA
 367 species, they share a commonality in that they are transcribed from DNA via the action of RNA
 368 polymerase. In the coming paragraphs, we will consider the synthesis of RNA as a rate limiting
 369 step in bacterial division by estimating how many RNA polymerases must be present to synthesize
 370 all necessary rRNA, mRNA, and tRNA.

371 rRNA

372 We begin with an estimation of the number of RNA polymerases needed to synthesize the rRNA
 373 that serve as catalytic and structural elements of the ribosome. Each ribosome contains three rRNA
 374 molecules of lengths 120, 1542, and 2904 nucleotides (BNID: 108093, **Milo et al. (2010)**). Thus, each
 375 ribosome consists of ≈ 4500 nucleotides. The *E. coli* RNA polymerase transcribes DNA to RNA at a
 376 rate of ≈ 40 nucleotides per second (BNID: 101904, **Milo et al. (2010)**). Thus, it takes a single RNA
 377 polymerase ≈ 100 s to synthesize the RNA needed to form a functional ribosome. Therefore, in a
 378 6000 s division time, a single RNA polymerase transcribing rRNA at a time would result in only \approx
 379 60 functional ribosomal rRNA units – far below the observed number of $\approx 10^4$ ribosomes per cell.

380 Of course, there can be more than one RNA polymerase transcribing at any given time. To eluci-
 381 date the *maximum* number of rRNA units that can be synthesized given a single copy of each rRNA
 382 gene, we will consider a hypothesis in which the rRNA operon is completely tiled with RNA poly-
 383 merase. How many polymerase could in principle fit on the rRNA operon? *In vivo* measurements
 384 of the kinetics of rRNA transcription have revealed that RNA polymerase are loaded onto the pro-
 385 moter of an rRNA gene at a rate of ≈ 1 per second (BNID: 111997; 102362, **Milo et al. (2010)**). If RNA
 386 polymerases are being constantly loaded on to the rRNA genes at this rate, then we can make the
 387 approximation that ≈ 1 functional rRNA unit is synthesized per second. With a 6000 second division
 388 time, this hypothesis leads to a maximal value of 6000 functional rRNA units, still undershooting
 389 the observed number of 10^4 ribosomes per cell.

390 *E. coli* has evolved a clever mechanism to surpass this kinetic limit for the rate of rRNA produc-
 391 tion. Rather than having only one copy of each rRNA gene, *E. coli* has seven copies of the operon
 392 (BNID: 100352, **Milo et al. (2010)**) all of which are localized near the origin of replication (**Birnbaum**
 393 **and Kaplan, 1971**). As fast growth requires that multiple copies are being synthesized simultane-
 394 ously, this means that the total number of rRNA genes can be on the order of $\approx 10 - 30$ at a given
 395 time (**Stevenson and Schmidt, 2004**). Using our standard time scale of a 6000 second division time,

396 we can make the lower-bound estimate that the typical cell will have 7 copies of the rRNA operon.
 397 Synthesizing one functional rRNA unit per second per operon, a total of 4×10^4 rRNA units can be
 398 synthesized, comfortably above the observed number of ribosomes per cell.

399 How many RNA polymerases are then needed to constantly transcribe 7 copies of the rRNA
 400 genes? We approach this estimate by considering the maximum number of RNA polymerases
 401 can be tiling the rRNA genes with a loading rate of 1 per second and a transcription rate of 40 nu-
 402 cleotides per second. Considering that a RNA polymerase has a physical footprint of approximately
 403 40 nucleotides (BNID: 107873, *Milo et al. (2010)*), we can state that there is ≈ 1 RNA polymerase
 404 per 80 nucleotides. With a total length of ≈ 4500 nucleotides per operon and 7 operons per well,
 405 the maximum number of RNA polymerases that can be transcribing rRNA at any given time is \approx
 406 400, setting a lower bound for the number of RNA polymerase required to make enough rRNA. As
 407 we will see in the coming sections, the synthesis of rRNA is the dominant requirement of the RNA
 408 polymerase pool.

409 mRNA

410 To form a functional protein, all protein coding genes must first be transcribed from DNA to form
 411 an mRNA molecule. While each protein requires an mRNA blueprint, many copies of the protein
 412 can be synthesized from a single mRNA. Factors such as strength of the ribosomal binding site,
 413 mRNA stability, and rare codon usage frequency dictate the number of proteins that can be made
 414 from a single mRNA, ranging from 10^1 to 10^4 (BNID: 104186; 100196; 106254, *Milo et al. (2010)*).
 415 Computing the geometric mean of this range yields ≈ 1000 proteins synthesized per mRNA, a value
 416 that emerges from quantitative measurements of the number of proteins per cell ($\approx 3 \times 10^6$, BNID:
 417 100088, *Milo et al. (2010)*) and total number of mRNA per cell ($\approx 3 \times 10^3$, BNID:100064, *Milo et al.*
 418 *(2010)*). In *E. coli*, the average protein is ≈ 300 amino acids in length (BNID: 108986; *Milo et al. (2010)*),
 419 meaning that the corresponding mRNA is ≈ 900 nucleotides which we will further approximate to
 420 be ≈ 1000 nucleotides given non-protein coding regions of the mRNA present on the 5' and 3' ends.
 421 With 3000 mRNA per cell, each around 1000 nucleotides in length, a total of 3×10^6 nucleotides
 422 must be linked together via RNA polymerase during transcription. With a 6000 second division
 423 time and a typical transcription rate of 40 nucleotides per second per polymerase, we arrive at a
 424 final estimate of ≈ 10 RNA polymerase complexes are necessary. This requirement is minuscule
 425 compared to the ≈ 400 polymerases needed to synthesize the necessary pool of rRNA molecules.

426 tRNA

427 Our final class of RNA molecules worthy of quantitative consideration is the the pool of tRNAs used
 428 during translation to map codon sequence to amino acid identity. Unlike mRNA or rRNA, each in-
 429 dividual tRNA is remarkably short, ranging from 70 to 95 nucleotides each (BNID: 109645; 102340,
 430 *Milo et al. (2010)*). What they lack in length, they make up for in abundance. There are approxi-
 431 mately ≈ 3000 tRNA molecules present for each of the 20 amino acids (BNID: 105280, *Milo et al.*
 432 *(2010)*), although the precise copy number is dependent on the identity of the amino acid identity.
 433 Using these values, we make the estimate that $\approx 5 \times 10^6$ nucleotides are sequestered in tRNA per
 434 cell. Using a similar approach as for our estimate of mRNA copy number, the cell requires ≈ 20 RNA
 435 polymerases to polymerase these nucleotides in a 6000 second time window. This requirement,
 436 much like the requirement for mRNA synthesis, pales in comparison to the number of polymerases
 437 needed to generate the rRNA pool.

438 RNA Polymerase and σ -factor Abundance

439 These estimates, summarized in ?? (A), reveal that synthesis of rRNA is the dominant force dictating
 440 the number of RNA polymerases needed per cell. For completeness, we can use our estimates of \approx
 441 400, 10, and 20 RNA polymerases needed to synthesize the required number of rRNAs, mRNAs, and
 442 tRNAs, respectively, to state that the typical cell needs to maintain a pool of ≈ 500 RNA polymerases.
 443 As is revealed in ?? (B), this estimate (≈ 500) is about and an order of magnitude below the observed

444 number of RNA polymerase complexes per cell (≈ 5000).

445 Protein synthesis

446 Lastly, we turn our attention to the process of translation. So far in our various estimates there
 447 has been little to suggest any apparent limit to how fast a bacterium might divide under steady-
 448 state growth. Even in our examples of *E. coli* grown rapidly under different carbohydrate sources
 449 (*Figure 2(B)*), cells are able to utilize less preferred carbon sources by inducing the expression of
 450 additional membrane transporters and enzymes. [Maybe go into Hwa style resource allocation
 451 with references added]. In this respect, gross overexpression of a protein can lead to a reduction
 452 of the growth rate.

453 We can determine the translation-limited growth rate by noting that the total number of peptide
 454 bonds created as the cell doubles N_{aa} will be given by, $\tau \cdot r_t \cdot R$. Here, τ refers to the doubling time of
 455 the cell under steady-state growth, r_t is the maximum translation rate, and R is the average number
 456 of ribosomes in the cell. With the growth rate related to the cell doubling time by $\lambda = \ln(2)/\tau$, we
 457 can write the translation-limited growth rate as,

$$\lambda_{\text{translation-limited}} = \frac{\ln(2) \cdot r_t \cdot R}{N_{aa}}. \quad (1)$$

458 Alternatively, since N_{aa} is related to the total protein mass through the molecular weight of each
 459 protein, we can also consider the growth rate in terms of ribosomal mass fraction. This calculation
 460 is shown in *Figure 7(A)*. This allows us to rewrite the growth rate as,

$$\lambda_{\text{translation-limited}} \approx \frac{\ln(2) \cdot r_t}{L_R} \Phi_R, \quad (2)$$

461 where L_R is the total length in amino acids that make up a ribosome, and Φ_R is the ribosomal mass
 462 fraction. This is plotted as a function of ribosomal fraction Φ_R in *Figure 7(A)*, with a translation rate
 463 $r_t = 17 \text{ aa/s}$ and $L_R = 17 \text{ aa}$, which corresponds to the length in amino acids for all ribosomal subunits
 464 of the 50S and 30S complexes and elongation factor required for translation.

465 Perhaps the first thing to notice is that there is a maximum growth rate at about $\lambda \approx 6 \text{ hr}^{-1}$, or
 466 doubling time of about 7 minutes. This maximum growth rate can be viewed as an inherent speed
 467 limit due to the need for the cell to double the cell's entire ribosomal mass. Interestingly, this limit is
 468 independent of the absolute number of ribosomes, but rather is simply given by time to translate
 469 an entire ribosome, L_R/r_t . As shown in *Figure 7(B)*, we can reconcile this with the observation
 470 that in order to double the average number of ribosomes, each ribosome must produce a second
 471 ribosome. This is a process that cannot be parallelized further.

472 Since a cell consists of more than just ribosomes, we can see that for Φ_R in the range of about
 473 0.1 - 0.3, the maximum growth rate is in line with experimentally reported growth rates around
 474 0.5 - 2 hr^{-1} . Here we have implicitly assumed that translation proceeds randomly, without pref-
 475 erence between ribosomal or non-ribosomal mRNA, which appears reasonable. Importantly, in
 476 order for a cell to scale this limit set by Φ_R the cell must increase its ribosomal abundance, either
 477 by synthesizing more ribosomes or reducing the fraction of non-ribosomal proteins.

478 One additional point to note is that across different species of bacteria, cells do not decrease
 479 their ribosomal abundance to zero in the limit of poorer nutrient condition [CITE?]. Indeed, some
 480 organisms appear to have constant ribosomal abundance irrespective of their growth rate [NB:
 481 ask Griffin and figure out what organism this is]. From the perspective of a bacterium dealing with
 482 uncertain nutrient conditions, there is likely a benefit for the cell to maintain some relative frac-
 483 tion of ribosomes to support rapid growth as nutrient conditions improve. In addition, given their
 484 massive size at about 850 kDa, they may play an as-yet fully understood role as a crowding agent
 485 in cellular function *Delarue et al. (2018); Soler-Bistué et al. (2020)*. If we consider a scenario where
 486 nutrient conditions become poorer and poorer, there must be a regime where the cell has more
 487 ribosomes than it can utilize. While this perhaps suggests less import to the process of translation,

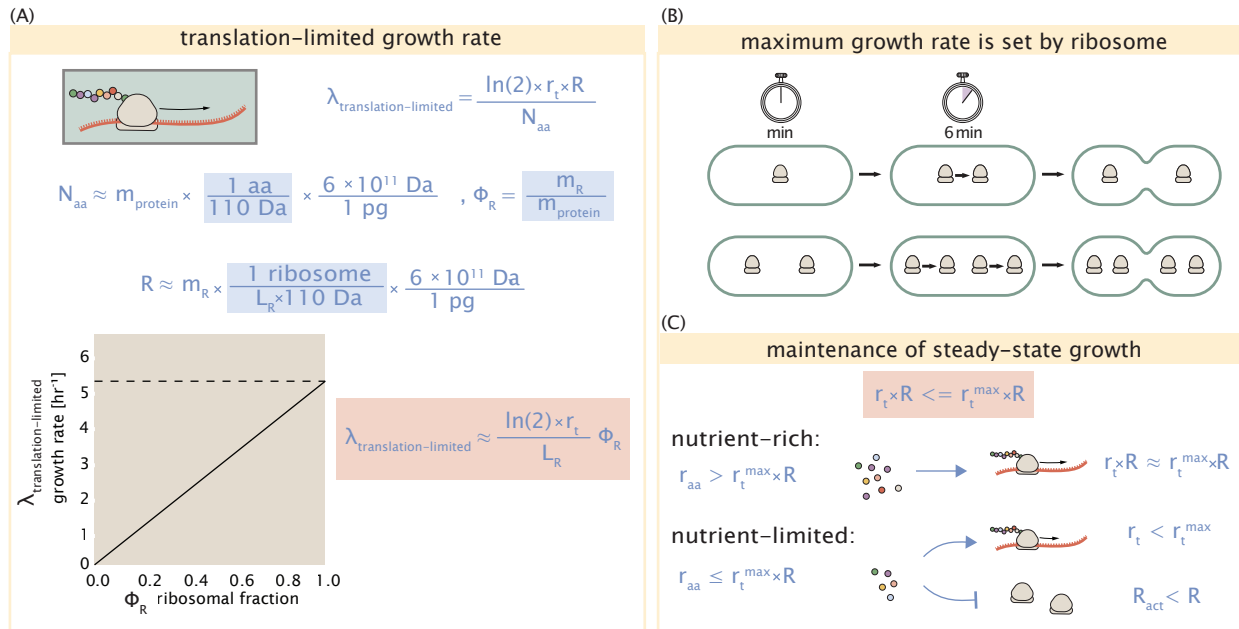


Figure 7. Translation-limited growth rate. (A) Here we consider the translation-limited growth as a function of ribosomal fraction. By mass balance, the time required to double the entire proteome (N_{aa} / r_t) sets the translation-limited growth rate, $\lambda_{\text{translation-limited}}$. Here N_{aa} is effectively the number of peptide bonds that must be translated, r_t is the translation elongation rate, and R is the number of ribosomes. This can also be re-written in terms of the ribosomal mass fraction $\Phi_R = m_R / m_{\text{protein}}$, where m_R is the total ribosomal mass and m_{protein} is the mass of all proteins in the cell. L_R refers to the summed length of the ribosome in amino acids. $\lambda_{\text{translation-limited}}$ is plotted as a function of Φ_R (solid line). (B) The dashed line in part (A) identifies a maximum growth rate that is set by the ribosome. Specifically, this growth rate corresponds to the time required to translate an entire ribosome, L_R / r_t . This is a result that is independent of the number of ribosomes in the cell as shown schematically here. (C)

Figure 8. . (A) (B) (C).

488 it is important to recognize that in order for a cell to maintain steady-state growth, the cell's transla-
 489 tion capacity must be mitigated. Otherwise, ribosomes will deplete their supply of amino acids and
 490 this will bring translation and cell growth to a halt (**Figure 7(C)**). We will consider the consequences
 491 of this in the case of *E. coli* next.

492 **Multiple replication forks provide one strategy to support faster growth.**

493 We now turn to our proteomic data from *E. coli* and plot the ribosomal fraction as a function of
 494 reported growth rate. Here we find that the ribosomal fraction always increases with growth rate.
 495 This is consistent with the behavior expected for *E. coli*, and an observation of intense study related
 496 to the so-called nutrient-limited growth law. In terms of absolute ribosomal abundance, we find
 497 that cells increase both their quantity and cellular concentration at faster growth.

498 One feature of *E. coli*, as well as other bacteria like *B. subtilis*, is the ability to begin replication of
 499 multiple copies of its genome during a single cell cycle. This is achieved through multiple initiation
 500 forks and nested DNA replication. [Need to refer to work from Jun lab here!! - under adder
 501 mechanism, the cell appears to add a certain cell mass in proportion to its number of origins]. We
 502 find that the ribosome copy number increases in proportion to the expected number of origins.
 503 The process of nested DNA replication will lead to a bias in gene dosage for genes closer to the
 504 origin of replication () Importantly, ribosomal protein and rRNA genes are closer to the origin of
 505 replication *Scholz et al. (2019)* and this provides a natural way for *E. coli* to bias the proportion
 506 of ribosomes at faster growth without the advent of additional gene regulation strategies. Given
 507 that ribosomal genes in *E. coli* appear to be transcribed at their maximal rate at fast growth rates
 508 [cite??], increasing ribosomal copy number through increased gene dosage represents a creative
 509 approach for the cell to grow faster without gross down-regulation of non-ribosomal genes.

510 **References**

- 511 Adelberg, G., Towbin, B. D., Rothschild, D., Dekel, E., Bren, A., and Alon, U. (2014). Hierarchy of non-glucose
 512 sugars in *Escherichia coli*. *BMC Systems Biology*, 8(1):133.
- 513 Antonenko, Y. N., Pohl, P., and Denisov, G. A. (1997). Permeation of ammonia across bilayer lipid membranes
 514 studied by ammonium ion selective microelectrodes. *Biophysical Journal*, 72(5):2187–2195.
- 515 Ashburner, M., Ball, C. A., Blake, J. A., Botstein, D., Butler, H., Cherry, J. M., Davis, A. P., Dolinski, K., Dwight, S. S.,
 516 Eppig, J. T., Harris, M. A., Hill, D. P., Issel-Tarver, L., Kasarskis, A., Lewis, S., Matese, J. C., Richardson, J. E.,
 517 Ringwald, M., Rubin, G. M., and Sherlock, G. (2000). Gene Ontology: tool for the unification of biology. *Nature Genetics*, 25(1):25–29.
- 518 Ason, B., Bertram, J. G., Hingorani, M. M., Beechem, J. M., O'Donnell, M., Goodman, M. F., and Bloom, L. B.
 519 (2000). A Model for *Escherichia coli* DNA Polymerase III Holoenzyme Assembly at Primer/Template Ends:
 520 DNA Triggers A Change In Binding Specificity of the γ Complex Clamp Loader. *Journal of Biological Chemistry*,
 521 275(4):3006–3015.
- 522 Assentoft, M., Kaptan, S., Schneider, H.-P., Deitmer, J. W., de Groot, B. L., and MacAulay, N. (2016). Aquaporin 4
 523 as a NH₃ Channel. *Journal of Biological Chemistry*, 291(36):19184–19195.
- 524 Basan, M., Zhu, M., Dai, X., Warren, M., Sévin, D., Wang, Y.-P., and Hwa, T. (2015). Inflating bacterial cells by
 525 increased protein synthesis. *Molecular Systems Biology*, 11(10):836.
- 526 Bauer, S. and Ziv, E. (1976). Dense growth of aerobic bacteria in a bench-scale fermentor. *Biotechnology and
 527 Bioengineering*, 18(1):81–94. _eprint: <https://onlinelibrary.wiley.com/doi/10.1002/bit.260180107>.
- 528 Belliveau, N. M., Barnes, S. L., Ireland, W. T., Jones, D. L., Sweredoski, M. J., Moradian, A., Hess, S., Kinney, J. B.,
 529 and Phillips, R. (2018). Systematic approach for dissecting the molecular mechanisms of transcriptional
 530 regulation in bacteria. *Proceedings of the National Academy of Sciences*, 115(21):E4796–E4805.
- 531

- 532 Birnbaum, L. S. and Kaplan, S. (1971). Localization of a Portion of the Ribosomal RNA Genes in *Escherichia coli*.
 533 *Proceedings of the National Academy of Sciences*, 68(5):925–929.
- 534 Booth, I. R., Mitchell, W. J., and Hamilton, W. A. (1979). Quantitative analysis of proton-linked transport systems.
 535 The lactose permease of *Escherichia coli*. *Biochemical Journal*, 182(3):687–696.
- 536 Cox, G. B., Newton, N. A., Gibson, F., Snoswell, A. M., and Hamilton, J. A. (1970). The function of ubiquinone in
 537 *Escherichia coli*. *Biochemical Journal*, 117(3):551–562.
- 538 Delarue, M., Brittingham, G. P., Pfeffer, S., Surovtsev, I. V., Pinglay, S., Kennedy, K. J., Schaffer, M., Gutierrez,
 539 J. I., Sang, D., Poterewicz, G., Chung, J. K., Plitzko, J. M., Groves, J. T., Jacobs-Wagner, C., Engel, B. D., and Holt,
 540 L. J. (2018). mTORC1 Controls Phase Separation and the Biophysical Properties of the Cytoplasm by Tuning
 541 Crowding. *Cell*, 174(2):338–349.e20.
- 542 Escalante, A., Salinas Cervantes, A., Gosset, G., and Bolívar, F. (2012). Current knowledge of the *Escherichia coli*
 543 phosphoenolpyruvate–carbohydrate phosphotransferase system: Peculiarities of regulation and impact on
 544 growth and product formation. *Applied Microbiology and Biotechnology*, 94(6):1483–1494.
- 545 Feist, A. M., Henry, C. S., Reed, J. L., Krummenacker, M., Joyce, A. R., Karp, P. D., Broadbelt, L. J., Hatzimanikatis,
 546 V., and Palsson, B. Ø. (2007). A genome-scale metabolic reconstruction for *Escherichia coli* K-12 MG1655 that
 547 accounts for 1260 ORFs and thermodynamic information. *Molecular Systems Biology*, 3(1):121.
- 548 Fijalkowska, I. J., Schaaper, R. M., and Jonczyk, P. (2012). DNA replication fidelity in *Escherichia coli*: A multi-DNA
 549 polymerase affair. *FEMS Microbiology Reviews*, 36(6):1105–1121.
- 550 Gama-Castro, S., Salgado, H., Santos-Zavaleta, A., Ledezma-Tejeida, D., Muñiz-Rascado, L., García-Sotelo, J. S.,
 551 Alquicira-Hernández, K., Martínez-Flores, I., Pannier, L., Castro-Mondragón, J. A., Medina-Rivera, A., Solano-
 552 Lira, H., Bonavides-Martínez, C., Pérez-Rueda, E., Alquicira-Hernández, S., Porrón-Sotelo, L., López-Fuentes,
 553 A., Hernández-Koutoucheva, A., Moral-Chávez, V. D., Rinaldi, F., and Collado-Vides, J. (2016). RegulonDB
 554 version 9.0: High-level integration of gene regulation, coexpression, motif clustering and beyond. *Nucleic
 555 Acids Research*, 44(D1):D133–D143.
- 556 Ge, J., Yu, G., Ator, M. A., and Stubbe, J. (2003). Pre-Steady-State and Steady-State Kinetic Analysis of *E. coli* Class
 557 I Ribonucleotide Reductase. *Biochemistry*, 42(34):10071–10083.
- 558 Harris, L. K. and Theriot, J. A. (2018). Surface Area to Volume Ratio: A Natural Variable for Bacterial Morphogen-
 559 esis. *Trends in microbiology*, 26(10):815–832.
- 560 Harris, R. M., Webb, D. C., Howitt, S. M., and Cox, G. B. (2001). Characterization of PitA and PitB from *Escherichia
 561 coli*. *Journal of Bacteriology*, 183(17):5008–5014.
- 562 Heldal, M., Norland, S., and Tumyr, O. (1985). X-ray microanalytic method for measurement of dry matter and
 563 elemental content of individual bacteria. *Applied and Environmental Microbiology*, 50(5):1251–1257.
- 564 Henkel, S. G., Beek, A. T., Steinsiek, S., Stagge, S., Bettenbrock, K., de Mattos, M. J. T., Sauter, T., Sawodny, O.,
 565 and Ederer, M. (2014). Basic Regulatory Principles of *Escherichia coli*'s Electron Transport Chain for Varying
 566 Oxygen Conditions. *PLoS ONE*, 9(9):e107640.
- 567 Hui, S., Silverman, J. M., Chen, S. S., Erickson, D. W., Basan, M., Wang, J., Hwa, T., and Williamson, J. R. (2015).
 568 Quantitative proteomic analysis reveals a simple strategy of global resource allocation in bacteria. *Molecular
 569 Systems Biology*, 11(2):e784–e784.
- 570 Ingledew, W. J. and Poole, R. K. (1984). The respiratory chains of *Escherichia coli*. *Microbiological Reviews*,
 571 48(3):222–271.
- 572 Ireland, W. T., Beeler, S. M., Flores-Bautista, E., Belliveau, N. M., Sweredoski, M. J., Moradian, A., Kinney, J. B.,
 573 and Phillips, R. (2020). Deciphering the regulatory genome of *Escherichia coli*, one hundred promoters at a
 574 time. *bioRxiv*.
- 575 Jacob, F. and Monod, J. (1961). Genetic regulatory mechanisms in the synthesis of proteins. *Journal of Molecular
 576 Biology*, 3(3):318–356.
- 577 Jun, S., Si, F., Pugatch, R., and Scott, M. (2018). Fundamental principles in bacterial physiology - history, recent
 578 progress, and the future with focus on cell size control: A review. *Reports on Progress in Physics*, 81(5):056601.
- 579 Khademi, S., O'Connell, J., Remis, J., Robles-Colmenares, Y., Miercke, L.J.W., and Stroud, R. M. (2004). Mechanism
 580 of Ammonia Transport by Amt/MEP/Rh: Structure of AmtB at 1.35 Å. *Science*, 305(5690):1587–1594.

- 581 Khademian, M. and Imlay, J. A. (2017). *Escherichia Coli* cytochrome c peroxidase is a respiratory oxidase that
582 enables the use of hydrogen peroxide as a terminal electron acceptor. *Proceedings of the National Academy
583 of Sciences*, 114(33):E6922–E6931.
- 584 Li, G.-W., Burkhardt, D., Gross, C., and Weissman, J. S. (2014). Quantifying absolute protein synthesis rates
585 reveals principles underlying allocation of cellular resources. *Cell*, 157(3):624–635.
- 586 Liu, M., Durfee, T., Cabrera, J. E., Zhao, K., Jin, D. J., and Blattner, F. R. (2005). Global Transcriptional Programs
587 Reveal a Carbon Source Foraging Strategy by *Escherichia coli*. *Journal of Biological Chemistry*, 280(16):15921–
588 15927.
- 589 Milo, R., Jorgensen, P., Moran, U., Weber, G., and Springer, M. (2010). BioNumbers—the database of key num-
590 bers in molecular and cell biology. *Nucleic Acids Research*, 38(suppl_1):D750–D753.
- 591 Monod, J. (1947). The phenomenon of enzymatic adaptation and its bearings on problems of genetics and
592 cellular differentiation. *Growth Symposium*, 9:223–289.
- 593 Neidhardt, F. C., Ingraham, J., and Schaechter, M. (1991). *Physiology of the Bacterial Cell - A Molecular Approach*,
594 volume 1. Elsevier.
- 595 Ojkic, N., Serbanescu, D., and Banerjee, S. (2019). Surface-to-volume scaling and aspect ratio preservation in
596 rod-shaped bacteria. *eLife*, 8:642.
- 597 Peebo, K., Valgepea, K., Maser, A., Nahku, R., Adamberg, K., and Vilu, R. (2015). Proteome reallocation in *Es-
598 cherichia coli* with increasing specific growth rate. *Molecular BioSystems*, 11(4):1184–1193.
- 599 Phillips, R. (2018). Membranes by the Numbers. In *Physics of Biological Membranes*, pages 73–105. Springer,
600 Cham, Cham.
- 601 Ramos, S. and Kaback, H. R. (1977). The relation between the electrochemical proton gradient and active trans-
602 port in *Escherichia coli* membrane vesicles. *Biochemistry*, 16(5):854–859.
- 603 Rosenberg, H., Gerdes, R. G., and Chegwidden, K. (1977). Two systems for the uptake of phosphate in *Es-
604 cherichia coli*. *Journal of Bacteriology*, 131(2):505–511.
- 605 Rudd, S. G., Valerie, N. C. K., and Helleday, T. (2016). Pathways controlling dNTP pools to maintain genome
606 stability. *DNA Repair*, 44:193–204.
- 607 Sánchez-Romero, M. A., Molina, F., and Jiménez-Sánchez, A. (2011). Organization of ribonucleoside diphosphate
608 reductase during multifork chromosome replication in *Escherichia coli*. *Microbiology*, 157(8):2220–2225.
- 609 Schaechter, M., MaalØe, O., and Kjeldgaard, N. O. (1958). Dependency on Medium and Temperature of Cell Size
610 and Chemical Composition during Balanced Growth of *Salmonella typhimurium*. *Microbiology*, 19(3):592–606.
- 611 Schmidt, A., Kochanowski, K., Vedelaar, S., Ahrné, E., Volkmer, B., Callipo, L., Knoops, K., Bauer, M., Aebersold,
612 R., and Heinemann, M. (2016). The quantitative and condition-dependent *Escherichia coli* proteome. *Nature
613 Biotechnology*, 34(1):104–110.
- 614 Scholz, S. A., Diao, R., Wolfe, M. B., Fivenson, E. M., Lin, X. N., and Freddolino, P. L. (2019). High-Resolution
615 Mapping of the *Escherichia coli* Chromosome Reveals Positions of High and Low Transcription. *Cell Systems*,
616 8(3):212–225.e9.
- 617 Scott, M., Gunderson, C. W., Mateescu, E. M., Zhang, Z., and Hwa, T. (2010). Interdependence of cell growth and
618 gene expression: origins and consequences. *Science*, 330(6007):1099–1102.
- 619 Sekowska, A., Kung, H.-F., and Danchin, A. (2000). Sulfur Metabolism in *Escherichia coli* and Related Bacteria:
620 Facts and Fiction. *Journal of Molecular Microbiology and Biotechnology*, 2(2):34.
- 621 Si, F., Le Treut, G., Sauls, J. T., Vadia, S., Levin, P. A., and Jun, S. (2019). Mechanistic Origin of Cell-Size Control
622 and Homeostasis in Bacteria. *Current Biology*, 29(11):1760–1770.e7.
- 623 Si, F., Li, D., Cox, S. E., Sauls, J. T., Azizi, O., Sou, C., Schwartz, A. B., Erickstad, M. J., Jun, Y., Li, X., and Jun, S. (2017).
624 Invariance of Initiation Mass and Predictability of Cell Size in *Escherichia coli*. *Current Biology*, 27(9):1278–
625 1287.
- 626 Sirko, A., Zatyka, M., Sadowy, E., and Hulanicka, D. (1995). Sulfate and thiosulfate transport in *Escherichia coli* K-
627 12: Evidence for a functional overlapping of sulfate- and thiosulfate-binding proteins. *Journal of Bacteriology*,
628 177(14):4134–4136.

- 629 Soler-Bistué, A., Aguilar-Pierlé, S., García-Garcéá, M., Val, M.-E., Sismeiro, O., Varet, H., Sieira, R., Krin, E., Skov-
630 gaard, O., Comerci, D.J., Eduardo P. C. Rocha, and Mazel, D. (2020). Macromolecular crowding links ribosomal
631 protein gene dosage to growth rate in *Vibrio cholerae*. *BMC Biology*, 18(1):1–18.
- 632 Stasi, R., Neves, H. I., and Spira, B. (2019). Phosphate uptake by the phosphonate transport system PhnCDE.
633 *BMC Microbiology*, 19.
- 634 Stevenson, B. S. and Schmidt, T. M. (2004). Life History Implications of rRNA Gene Copy Number in *Escherichia*
635 *coli*. *Applied and Environmental Microbiology*, 70(11):6670–6677.
- 636 Stouthamer, A. H. and Bettenhaussen, C. W. (1977). A continuous culture study of an ATPase-negative mutant
637 of *Escherichia coli*. *Archives of Microbiology*, 113(3):185–189.
- 638 Szenk, M., Dill, K. A., and de Graff, A. M. R. (2017). Why Do Fast-Growing Bacteria Enter Overflow Metabolism?
639 Testing the Membrane Real Estate Hypothesis. *Cell Systems*, 5(2):95–104.
- 640 Tatusov, R. L., Galperin, M. Y., Natale, D. A., and Koonin, E. V. (2000). The COG database: a tool for genome-scale
641 analysis of protein functions and evolution. *Nucleic Acids Research*, 28(1):33–36.
- 642 Taymaz-Nikerel, H., Borujeni, A. E., Verheijen, P. J. T., Heijnen, J. J., and van Gulik, W. M. (2010).
643 Genome-derived minimal metabolic models for *Escherichia coli* MG1655 with estimated in
644 vivo respiratory ATP stoichiometry. *Biotechnology and Bioengineering*, 107(2):369–381. _eprint:
645 <https://onlinelibrary.wiley.com/doi/pdf/10.1002/bit.22802>.
- 646 The Gene Ontology Consortium (2018). The Gene Ontology Resource: 20 years and still GOing strong. *Nucleic
647 Acids Research*, 47(D1):D330–D338.
- 648 Valgepea, K., Adamberg, K., Seiman, A., and Vilu, R. (2013). *Escherichia coli* achieves faster growth by increasing
649 catalytic and translation rates of proteins. *Molecular BioSystems*, 9(9):2344.
- 650 van Heeswijk, W. C., Westerhoff, H. V., and Boogerd, F. C. (2013). Nitrogen Assimilation in *Escherichia coli*: Putting
651 Molecular Data into a Systems Perspective. *Microbiology and Molecular Biology Reviews*, 77(4):628–695.
- 652 Weber, J. and Senior, A. E. (2003). ATP synthesis driven by proton transport in F1F0-ATP synthase. *FEBS Letters*,
653 545(1):61–70.
- 654 Willsky, G. R., Bennett, R. L., and Malamy, M. H. (1973). Inorganic Phosphate Transport in *Escherichia coli*:
655 Involvement of Two Genes Which Play a Role in Alkaline Phosphatase Regulation. *Journal of Bacteriology*,
656 113(2):529–539.
- 657 Zhang, L., Jiang, W., Nan, J., Almqvist, J., and Huang, Y. (2014a). The *Escherichia coli* CysZ is a pH dependent
658 sulfate transporter that can be inhibited by sulfite. *Biochimica et Biophysica Acta (BBA) - Biomembranes*,
659 1838(7):1809–1816.
- 660 Zhang, Z., Aboulwafa, M., and Saier, M. H. (2014b). Regulation of crp gene expression by the catabolite repres-
661 sor/activator, cra, in *Escherichia coli*. *Journal of Molecular Microbiology and Biotechnology*, 24(3):135–141.